Original Research Article

Crack-growth on canvas paintings during transport simulation monitored with digital holographic speckle interferometry

ABSTRACT

Transportation effects are of prime importance for the deterioration mechanisms that disintegrate the structural condition of movable painted artworks. Cracking is most common result of intense transportation and most common cause of reduced state of conservation. In this study two realistic conditions are encountered in the laboratory to simulate transportation effects: A transport simulator that reproduces real transportation vibrations and a high resolution technique that monitors in real time the surface response. The measurements were carried out on canvas samples with known defects. Results are encouraging for significant assessment of transportation effects in crack growth and propagation studies through real time monitoring of canvas surface.

Keywords: Canvas, transportation, holography interferometry, digital holography speckle pattern interferometry

1. INTRODUCTION

Fragile canvas paintings subjected to transportation during a loan for exhibition may return in a worse state due to adverse conditions while travelling [1]. Transportation including handling of freight at ports and airports, vehicles on bumpy roads and trolleys are associated with considerable risks for the canvases. The issues arising from transportation refer to the direct impact on the artworks, the methods to assess this impact and also to the contrivance of new approaches to prevent the damages [2]. Though a lot of work has been done on the ambient conditions (i.e. temperature and relative humidity) [3,4], not much work has taken place on the vibration and shock during transportation. Studies of early 1990s have recorded the impact of vibration and mishandling with photography and natural frequency measurements of canvas as well as acceleration measurements with attached accelerometers [5-8]. An electrohydraulic shaker applying random vibration had also been developed in the same period to test canvases in the laboratory [9]. Thus, the output of the measurements was mainly acceleration data. Later on, commercial sensors have been developed in order to record the oscillation characteristics of vibration and shock during transportation while other sensors more simple prove the event of a mishandling or the application of a critical frequency. Recent work has indirectly estimated the strain of real canvas paintings during transportation and handling by the use of triangulation laser displacement sensors [10]. In order to document the impact of transportation (i.e. mechanical damages, cracks, detachments etc.), conventional methods such as visual examination, raking light or microscopy are applied by conservators. A non conventional method, for conservation, developed to predict crack creation and growth, through computer generated strain field, is finite element analysis using computer simulated models [11]. The main problem though remains that the impact of vibration of composite objects like artworks, under real travelling conditions is very difficult to be assessed and predicted.

Non contact laser techniques that have been used in the topic of structural documentation of canvas, from high to moderate resolution, are optical coherence tomography [12], coherent digital holographic interferometry [13] photorefractive holography and shearography [14,15] but they were not used for assessing the impact of vibration loadings so far. Furthermore, the critical level of tolerable strains induced by vibration quoted in the literature are based on fatigue research dealing with modern construction materials which has been applied also on painting materials [7]. This paper aims to record the vibration impact during the process of generation of cracking thus to record the impact of vibration in real time [16]

The state of the art up to date refers mainly to the study of vibrating surfaces while the recording process registers the vibrational modes of the examined canvases. This approach does not allow thorough crack-generation studies. Thus we reconsider our approach and instead of recording the vibrating surface at the moment of the vibration (direct vibration effect) we record the impact on the artwork itself during transportation. The vibration impact on canvas is the factor to connect the real conditions of transportation to mechanisms of fatigue and failure of the layers and materials consisting painted canvases. Vibration forces canvases to random motion or resonate local structural faults generating inhomogeneous distribution of stresses among the frame and the vibrating membrane of canvas. Stressed areas in turn generate deformation or fracture or pulverization depending on the vibration characteristics, the materials, their cohesion as well as ageing factors. Repeated vibration cycles exceeding the elasticity threshold of fatigue level deteriorate the invisible structural problems and lead to progressive plasticity limits associated with the structural failure and cracking caused by accumulative fatigue. From the instant that the adhesion of materials is getting loose and degenerates to invisible micro-cracks till they grow and interconnect and become visible to the naked eye, it is a continuous process. Being able to monitor the canvas reactions to fatigue process that progressively or abruptly leads to failure is an essential step to the understanding and interpretation of the destructive mechanisms due to vibration.

To record the impact of transport and handling directly from an artwork we employed Digital Holographic Speckle Pattern Interferometry (DHSPI), widely used up to date in high resolution structural documentation and diagnosis of artworks [16-24]. To study in a systematic and controllable way the vibration impact the vibration conditions, as recorded during real transportation, were reproduced in the lab. The reproduction was feasible by a new transport simulator[1], that allows reproducible simulation of any transport logs on sample paintings in the laboratory. Monitoring interferometrically in real-time the realistic conditions has enabled the visualization of crack growth process on canvas. The study was made on new canvas painting samples subjected on consequent vibration cycles.

2. EXPERIMENTAL DESCRIPTION

2.1 Digital Holographic Speckle Pattern Interferometry (DHSPI)

A portable system based on geometry for digital holographic speckle pattern interferometry was implemented to illuminate remotely the canvas surface during the process of vibrating cycles in order to monitor the structural reactions [25]. The geometry is according to holographic interferometry principles that allow recording the phase variations of mutually coherent laser beams represented by beams carrying an object (O) and reference (R) field. The superposition of phase variations gives rise to macroscopic and thus visible interferometric fringes overlaid on object surface. Each fringe-pair describes a cosine distribution of light equal to half of the laser wavelength, λ. The total number of fringes corresponds to the magnitude of total surface displacement taking place during the deformation process of the surface. The technique is directly quantitative while the measurement unit of $^1/_2\lambda$ employed allows the recording of microscopic surface motion with high precision [26-29]. Another interesting point of the optical geometry is the unique property of sensitivity to x,y,z and especially the z-direction of displacement. Thus the DHSPI system registers the out-of-plane deformations that are due to the canvas response in the transportation frequencies without neglecting the in-plane stress at x,y due to common transportation punches.

The DHSPI system shown in figure 1, implements an optical head with a Nd:YAG Elforlight G4 laser as a light source with special characteristics: 250 mW at 532 nm, DPSS (Diode Pump Solid State), high spatial-temporal coherence with TEM:00 SLM (Single Longitudinal Mode) and a coherent length of 30 m for far access

[1] *Developed in the framework of CTI Project: "Transporting fragile paintings" (*www.gemaeldetransport.ch)

illumination to the target, and a CCD detector Basler A102f with resolution 1392H x 1040V and pixel size 6,45 μm x 6,45 μm as high resolution digital recording medium. The captured images are transferred to a PC using the Firewire 1394 protocol. The object's surface is recorded using the 5-frame algorithm, which uses two sets of five captured images separated at temporal windows of 10 sec at each set. The first set of images is captured using the π/2 phase difference in a relaxed state of the sample. The second set of images is captured using the π/2 phase difference in a displaced state following the induced surface displacement of the canvas, with unknown phase difference. Multiple sets of 5-frame images is captured and compared to the initial set. The metrological data provided by DHSPI is of the order of 266nm (λ laser wavelength) [29, 30].

2.2 Transport simulator

A transport simulator shown in figure 1 is built to simulate linear movement along a single axis with a maximum displacement of 70 mm. A maximum weight of 20 kg can be accelerated up to 50 m/s^2 along the x, y or z axis on the slider. This allows performing the simulation sequentially along each axis to achieve every translational degree of freedom. For this study the movement direction perpendicular to the sample was used. The control element (dSpace, DS1103) is capable of reproducing any logged vibration profiles captured during real transport monitoring as well as harmonic vibrations and bandwidth limited white noise. The movements on the sample painting are logged by a triaxial accelerometer (PCB 356A16) attached to the stretcher and a uniaxial accelerometer (PCB 352A73) mounted in the centre of the back. The placement of the uniaxial sensor was based on the ideal behavior of membranes. The highest amplitudes are expected in the centre of the canvas. The actual canvas displacement can be derived from the acceleration signals by appropriate numerical computations.

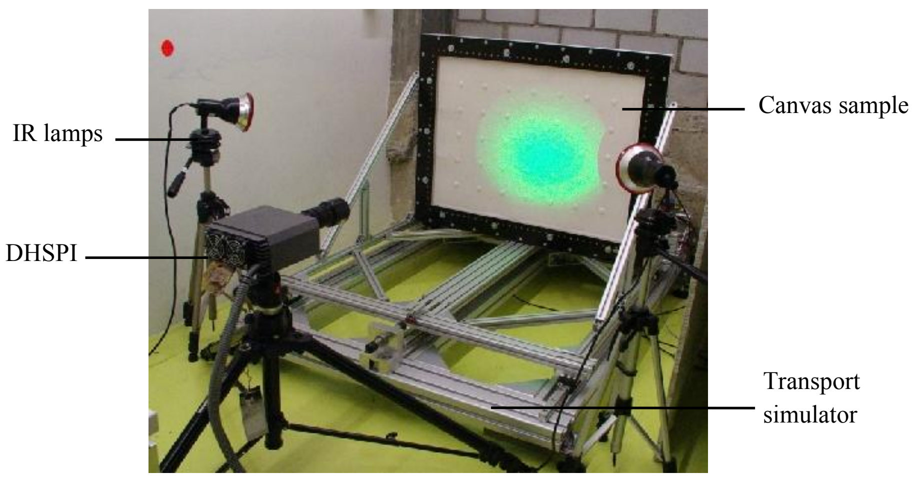

Figure 1 Photograph of the DHSPI monitoring system and transport simulator set up.

2.3 Samples and loading

2.3.1 First set of samples and loading

2.3.1.1 Samples

For the reproducibility of the experiments, canvas paintings with defined composition and layer thickness were produced as modeled samples. The first TP1 sample (Test Painting 1) support is a linen canvas, which was sized by brush with warm skin glue. Two layers of gesso serve as vulnerable paint layer. A partial black layer of acrylic paint was applied for optical contrast. Shellac and dammar were used for varnish. On the structure “weak” spots were integrated as known defects. In order to produce adhesion gaps between the sized support and the gesso layers Tricyclen- Camphen was used. Tricyclen-Camphen sublimes very fast. It was heated to 70°C and applied with a brush. The position of the weak spots is shown in Figure 2.

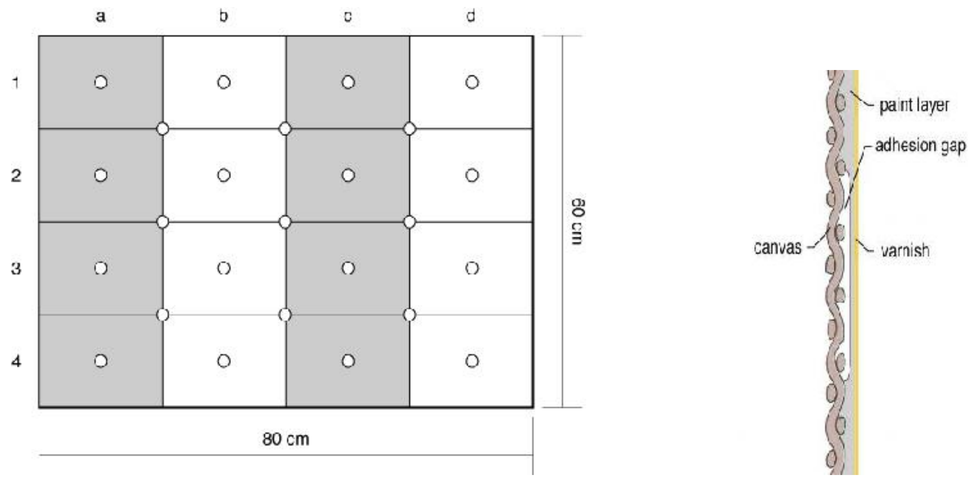

(a) (b)

Figure 2 (a) Schematic of a sample. Circles indicate the location of weak spots. (b) Schematic of the construction of the sample.

2.3.1.2 Vibration loading

Several types of real artwork transfers were logged with respect to shock and vibration emissions. The format of the logged paintings was medium to large. They were transported in specific climate cases with triaxial sensors mounted on the object and the protective case.

For the first set of experiments a random white noise with limited bandwidth (1 to 50 Hz) and variable amplitude was chosen as vibration loading.

2.3.2 Second set of samples and loading

2.3.2.1 Samples

The second set of samples were constructed by canvas supports also which were primed and painted with two layers of a gesso mixture made of chalk, gypsum and fish glue using a paintbrush. Two separate spots of weakness were integrated in the otherwise homogenous texture in order to concentrate mechanical forces (figure 3). Small weights (1.6g of gesso) were locally fixed to the surface with a grid of 10x10cm to cause centers of vibration. Zones with adhesion gaps were generated with a volatile intermediate layer of cyclododecan. These zones were of interest to study tensile stress within the gesso layer. In order to have the same paint layer thickness screen printing technique was modified. Test paintings named FG1, FG2, FG3 contain both kinds of fragile spots (F is for the fragile spots of the adhesion gaps and G is for the gesso weights). Samples dimensions are 80x60x(≈0.1-0.3) cm attached on a tensional frame.

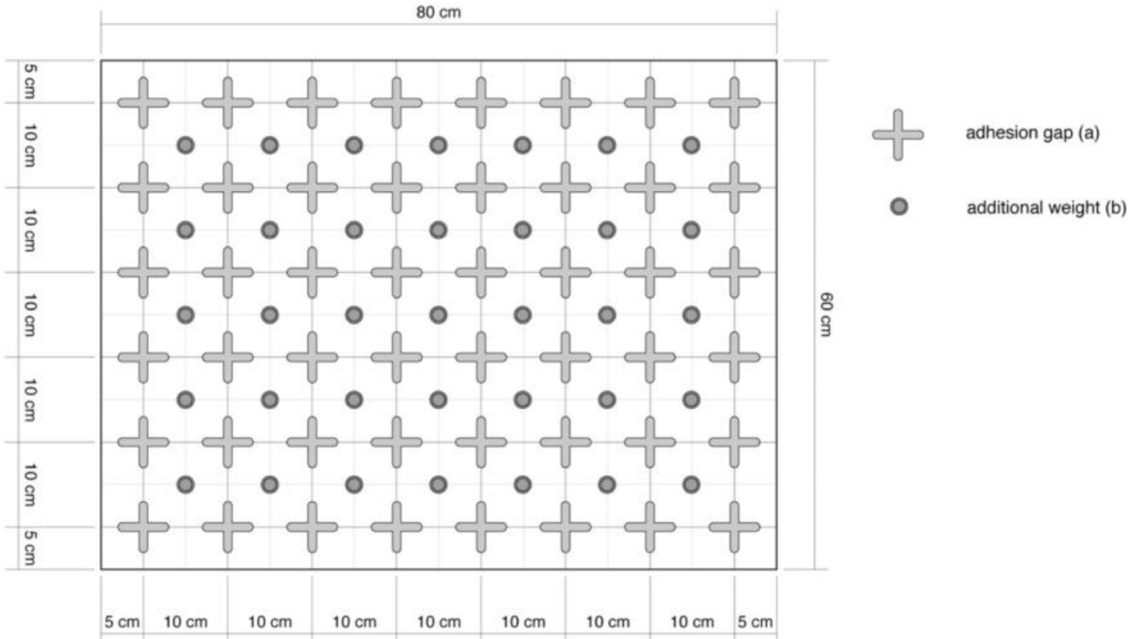

Figure 3 Schematic of canvas sample with known structural defects on the sample.

2.3.2.2 Vibration loading

The second set of experiments was based on an extract of the main shock and vibration events of the log profiles (figure 4). The 'truck' sequence thus culminates in 20sec of handling (loading/ unloading/ trolley) and 80sec of truck transport. For longer simulation the according profile has been looped. The root mean square (rms) of the whole profile is 2,14m/s^2, with a maximum acceleration of 28m/s^2.

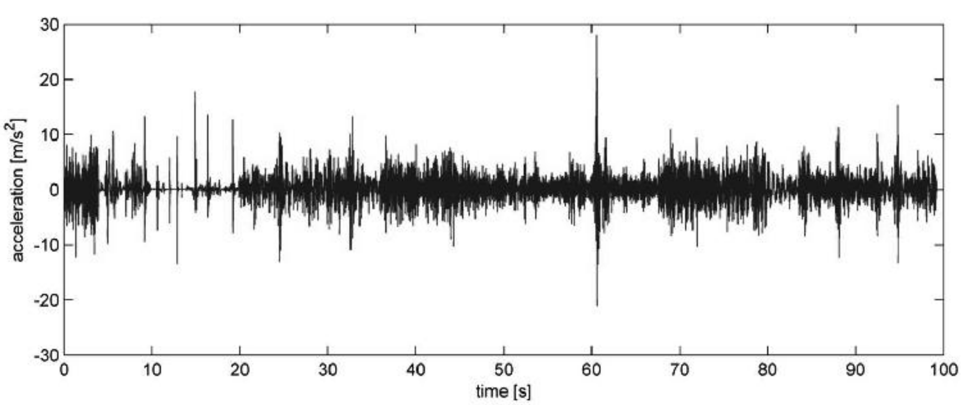

Figure 4 Vibration profile of rms = 2,14m/s^2.

2.4 Description of Experimental Procedure

The vibration loadings applied by the transport simulator and followed by DHSPI measurements took place as described in table 1. Before any vibration loading a reference DHSPI record was performed registering the structural condition of the sample and the induced defects before the vibration impact. To provoke displacement before vibration loading a thermal excitation was induced by two infrared lamps, placed in front of the sample in distance of 0,7m measured from the center of the sample. The induced temperature increase of the samples measured in the centre, reached maximum +3 ^{o}C. The recording head of DHSPI was at a distance of 1.30 m from the samples to achieve detailed visualisation measurements in the centre of the canvas. After the application of the first vibration load the surface displacement was recorded and the raw data was checked for possible vibration impact. Consecutive vibration loadings were successively monitored. In order to minimize environmental influence on the samples' reaction the laboratory conditions kept constantly stable.

Table 1 Experimental Procedure

STEP 1	1. Reference state registration 1.1 DHSPI measurement before any vibration cycle by thermal loading (with backboard)
STEP 2	2. Altered state registration 2.2 Vibration cycle (without backboard) 2.3 DHSPI measurement by thermal loading (with backboard) 2.4 Raw data check for visible crack creation and propagation
STEP 3	Repeating 2.2, 2.3, 2.4 as long is required

2.4.1 Methodology for crack monitoring via fringe pattern

The employed interference fringe formation process generates equidistant distribution of continuous field seen as dark and light zones overlaying the illuminated surface. Surface cracks are located by the break that cause in the fringe continuation. Subsurface cracks starting deeper inside between the interface of canvas and the overlaying painting layers are not causing break in fringe continuation unless they are affecting the illuminated surface. In such case provoke inconsistency in fringe formation process. To register both surface and subsurface cracks all the areas of inconsistencies in continuous field of fringes are registered and examined in each record. As the crack reaches the surface the fringe inconsistency becomes more apparent till fringes localising and sizing the crack appear as broken lines. The visual characteristic of the crack effect on the fringes of the interferogram is the "broken" or "dead-end" fringes [31-33]. The crack maps in this study are drawn by selecting the localized fringe interruptions manually by the aid of software; the length of each crack is defined by the length of interrupted fringes.

During series of monitoring a crack indication may appear occasionally in one interferogram or in few interferograms then another series of monitoring with another set of experimental parameters is applied to define better the crack location and size. When the crack appears constantly in sequence of interferograms, the location and size is steady and the crack interconnection and propagation is examined. This is performed by the determination of coordinates describing the full length each time. The coordinates to express a crack-length are scalar 'x' and 'y' measurements of planar objects. A crack map is produced using the full set of data of each monitored sequence of interferograms. Each interferogram records the physical differentiation due to the impact of the hidden cracks in respect to the illuminated surface.

At the time instant an interferogram is recorded not all the cracks necessarily provoke displacement at the surface to produce differentiation at the interferometric pattern covering the surface. Therefore some cracks, or even some parts of a crack depending on the position of the crack relevant to surface, remain hidden e.g. cracks running not parallel to surfaces but perpendicular or lying in angles. The intermittent appearance of cracks is common during surface relaxation from a loading and the first interferograms witness in most detail the structural condition including tracing of existent or inborn cracks. This initial time-frame of first interferograms formation represents a unique temporal response of any examined surface to the impact of loading. At the start of thermally induced dimensional changes defects show the highest spatial density values [34]. The thermal loading is a critical parameter for best visualization of structural condition in thermodynamically sensitive inhomogeneous composites [27]. In the measurements recorded here cracks appear with +2,5^{o}C applied thermal loading and with +3 ^{o}C at ΔT_1, ΔT_2, ΔT_3 etc. The thermal differentiation of a crack response makes its location distinguishable. Thus loading is applied in a gradual increasing procedure to ensure full detection of existent defect or crack.

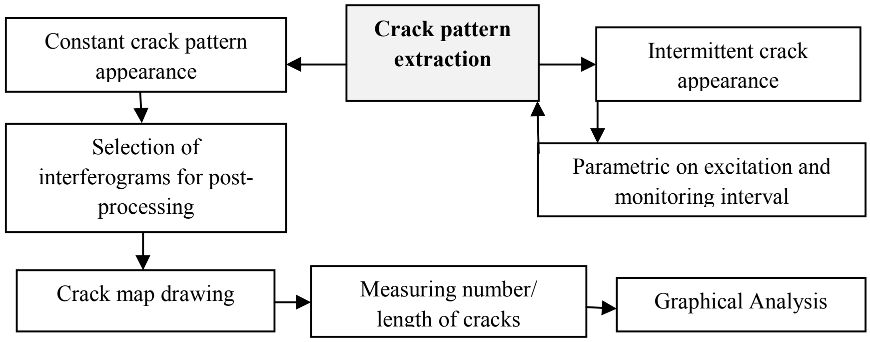

Figure 5 Schematic representation of the experimental measuring methodology.

3. RESULTS

3.1 First set of samples and loading

The first preliminary tests were carried out by applying twelve vibration cycles with a random white noise (1 to 50 Hz) and increasing acceleration amplitude starting at $1m/s^2$ (rms). The duration of each cycle was set to 10 seconds. In detail the description of the vibration cycles is shown in table 2. The upper limit of the transport simulator was $10m/s^2$. A characteristic crack map showing the one-dimensional length propagation is illustrated in figure 6. The exemplary crack pattern is generated among the adhesion gaps confirming the fracture theory of active connection among existed defects. The lower gap is not active yet and the theoretical models based on elastic media are not enough to predict time of activation since canvas is not considered isotropic. The first surface crack appeared after the 5th vibration cycle. No new cracks appeared after the 6th cycle and after the 8th cycle a sudden increase is shown. From 8th to 9th cycle the number of cracks is doubled. The best fit for the points of the diagram was made by an exponential curve described by the equation $y=e^{a+bx+cx2}$ (figure 7). As it is shown in the diagram of figure 7 it is quite clear that the experimental measurements of the total number of cracks after each vibration cycle are accordant with the theoretical exponential function.

Table 2 Vibration cycles applied on Test Painting 1

Number of vibration cycle	Acceleration Profile	RMS Acceleration	Duration
1	Noise 1-50Hz	$1m/s^2$	10s
2	Noise 1-50Hz	$2m/s^2$	10s
3	Noise 1-50Hz	$3m/s^2$	10s
4	Noise 1-50Hz	$4m/s^2$	10s
5	Noise 1-50Hz	$5m/s^2$	10s
6	Noise 1-50Hz	$6m/s^2$	10s
7	Noise 1-50Hz	$7m/s^2$	10s
8	Noise 1-50Hz	$8m/s^2$	10s
9	Noise 1-50Hz	$9m/s^2$	10s
10	Noise 1-50Hz	$10m/s^2$	10s

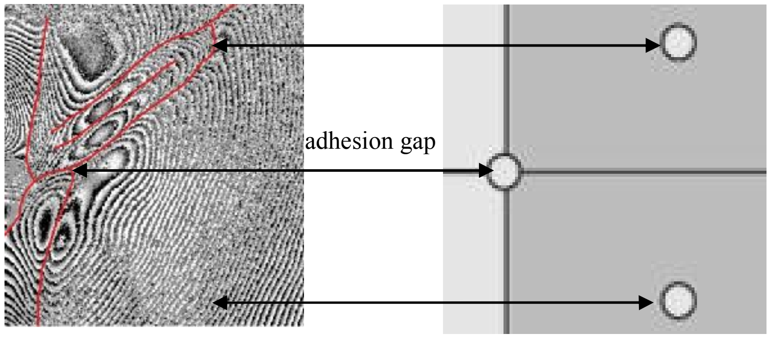

(a) (b)

Figure 6. Interferometric example of local crack map registered from interferograms after 10th vibration cycle at t=100 min compared to known induced defect map, in a) crack map resulted from interferograms of sample TP1, propagation length marked in red, and b) the known defect map.

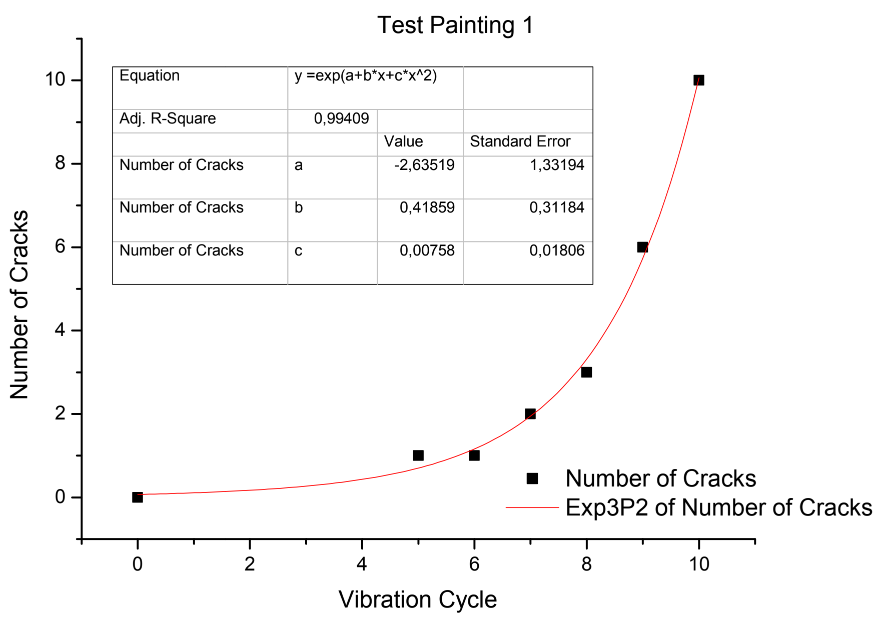

Figure 7 Total number of cracks measured after each vibration cycle. The crack growth is exponential.

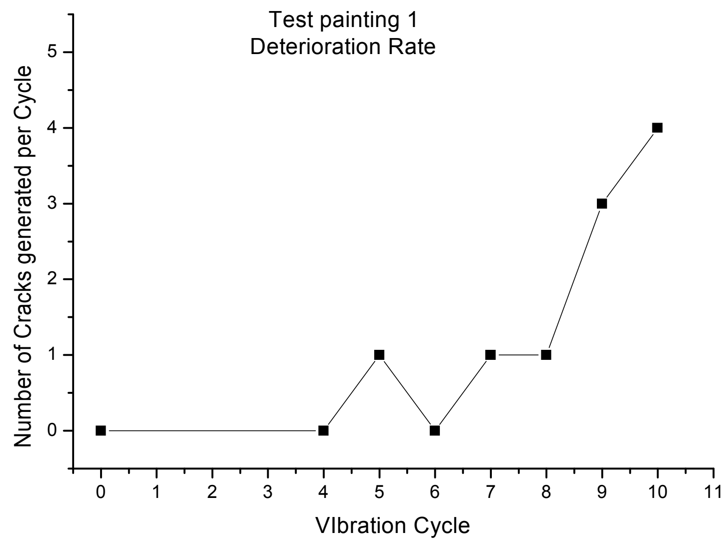

Figure 8 Deterioration rate of the test painting measured in number of new cracks generated after each vibration cycle.

The rate of deterioration, in terms of new cracks generated after each cycle, is illustrated in figure 8. It is at an experimental stable rate until the 8^{th} cycle with higher increase until the 10^{th} cycle. Each vibration cycle from 1-7 m/sec^2 rms generates new center of cracking deteriorating further the structural condition. The next five cycles from 8-9 m/sec^2 each worsen strongly the deterioration. Number of cracks can be measured in absolute terms through the qualitative examination of the crack patterns. It is also expected a higher number of cracks between the 8^{th} and the 10^{th} cycle as the applied root mean square acceleration reaches 8 to $10m/s^2$, considered as very high for transporting canvas paintings.

3.2 Second set of samples and loading

The second set of experiments (§ 2.3.2) carried out by applying a stable acceleration profile and a varying duration of each cycle. The detailed description of each vibration cycle for the three samples is shown in tables 3, 4 and 5.

Table 3 Vibration cycles applied on Test Painting FG1

Number of vibration cycle	Acceleration Profile	RMS Acceleration	Duration
1	LH	$2,14m/s^2$	30min
2	LH	$2,14m/s^2$	30min
3	LH	$2,14m/s^2$	30min
4	LH	$2,14m/s^2$	60min
5	LH	$2,14m/s^2$	60min
6	LH	$2,14m/s^2$	60min
7	LH	$2,14m/s^2$	60min
8	LH	$2,14m/s^2$	60min
9	LH	$2,14m/s^2$	120min
10	LH	$2,14m/s^2$	120min
11	LH	$2,14m/s^2$	120min
12	LH	$2,14m/s^2$	30min
13	LH	$2,14m/s^2$	30min
14	LH	$2,14m/s^2$	30min

Table 4 Vibration cycles applied on Test Painting FG2

Number of vibration cycle	Acceleration Profile	RMS Acceleration	Duration
1	LH	2,14m/s^2	30min
2	LH	2,14m/s^2	480min
3	LH	2,14m/s^2	60min
4	LH	2,14m/s^2	60min
5	LH	2,14m/s^2	60min
6	LH	2,14m/s^2	60min
7	LH	2,14m/s^2	60min
8	LH	2,14m/s^2	30min
9	LH	2,14m/s^2	30min

Table 5 Vibration cycles applied on Test Painting FG3

Number of vibration cycle	Acceleration Profile	RMS Acceleration	Duration
1	LH	2,14m/s^2	30min
2	LH	2,14m/s^2	230min
3	LH	2,14m/s^2	30min
4	LH	2,14m/s^2	30min
5	LH	2,14m/s^2	30min

The first two surface cracks on sample FG1 appeared after the 11th cycle and a total vibration time of 750min, while the next two appeared 60 min later at 810 min. In FG1 sample there were generated 6 cracks after 840 min in total and the last two cracks were formed only 30 min later at 840 min.
The first surface crack on sample FG2 appeared after the 7th cycle and a total vibration time of 810min, while the next crack appeared 30min later at 840 min (figure 9). In FG2 there were also 6 cracks after 870 min in total and the last four cracks were formed only 30min later at 870 min.

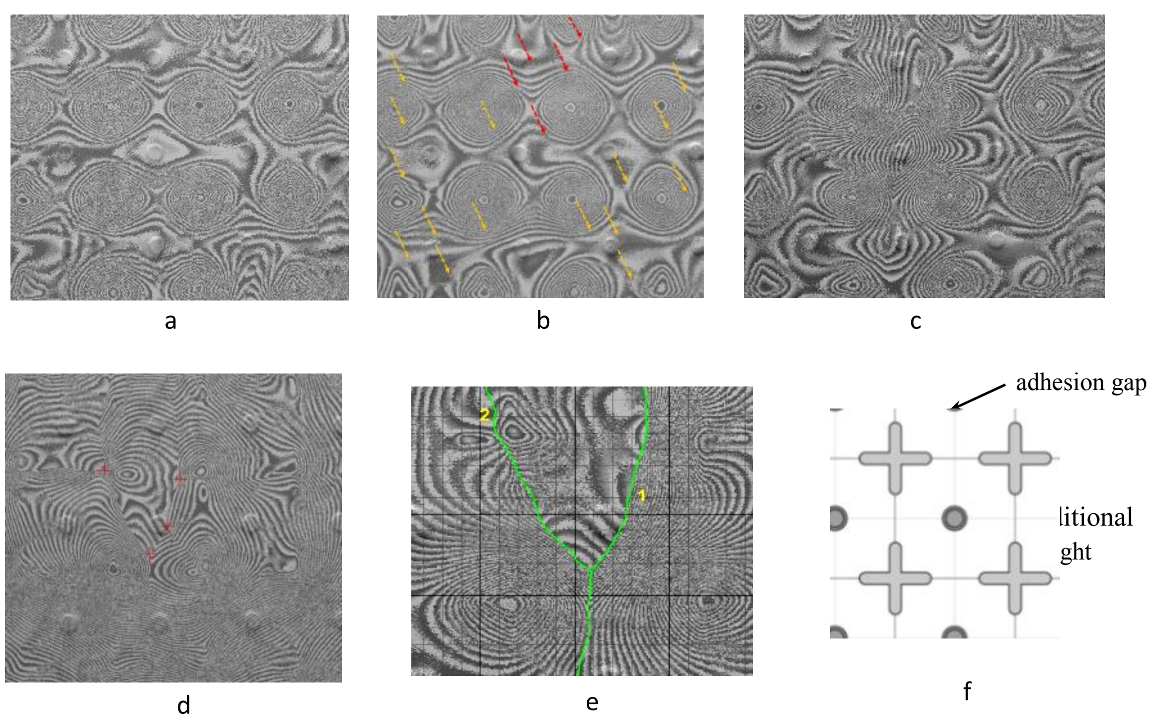

Figure 9 Example of interferograms, a) reference interferogram -before vibration loading- of sample FG2 according to the sample construction shown in figure 3, b) after 1st vibration cycle at t=30 min. Orange arrows show potential yet hidden cracks. Red arrow shows the first surface crack that appeared after 7th vibration cycle at t=810 min, c) with red arrows indicating the full length of the crack, d) FG2 after 9th vibration cycle and at t= 890 min, e) zoom-in surface crack map studied from interferograms of sample FG2 showing the first two surface cracks and f) zoom-in known defect map.

The first surface crack on sample FG3 appeared after the 2nd cycle and a total vibration time of 260min; faster compared to the previous samples. To verify if this fast response is within a statistical range another set of experiments and samples is planned.

The results from the above three samples in terms of the number of cracks after each cycle are illustrated in graphs of figures 10 and 11. It is noticeable that in all experiments and samples inborn yet hidden cracks are giving evidence of existence in the interferograms from the starting of the vibration loading cycles and tenths or hundreds of minutes before first surface crack appear.

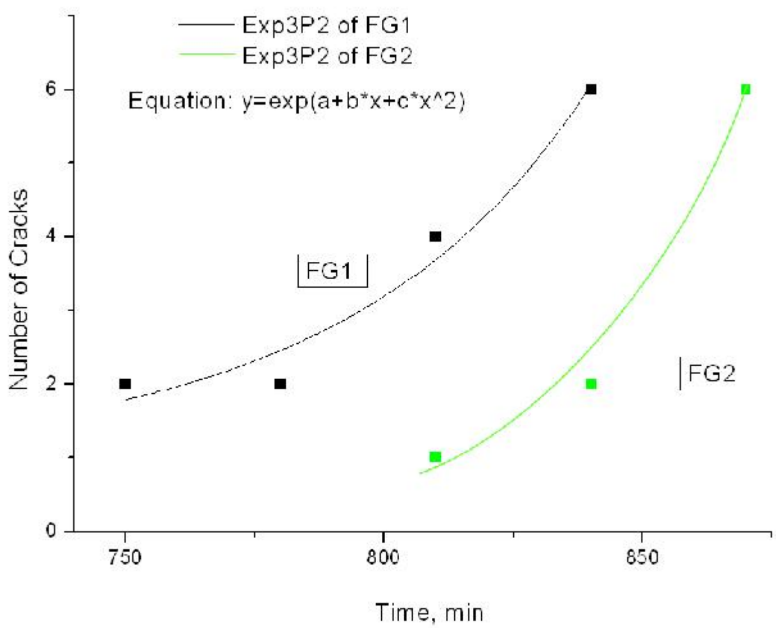

Figure 10 Number of surface cracks of samples FG1 and FG2 measured in time, after each vibration cycle. The growth of crack number is clearly exponential.

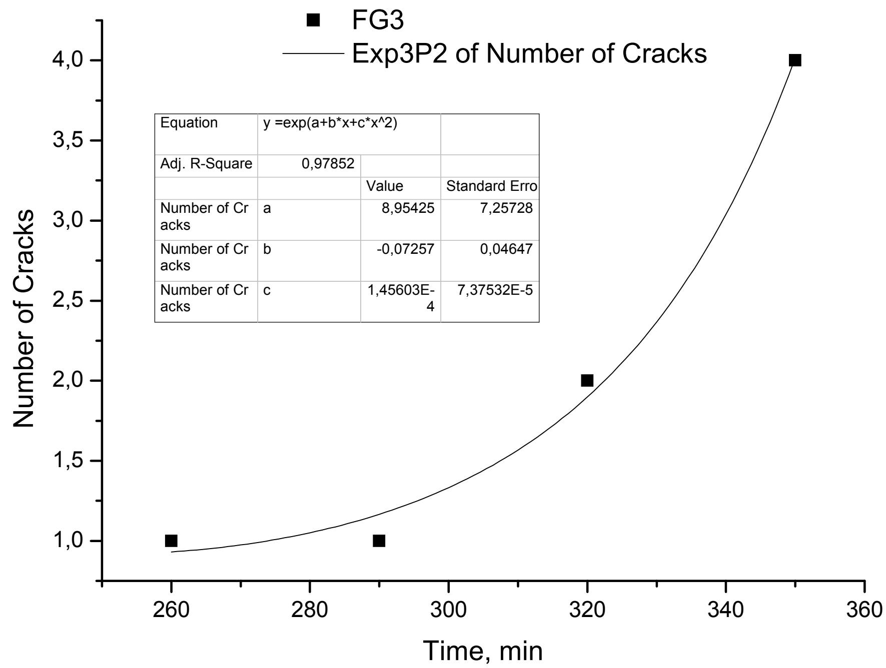

Figure 11 Number of surface cracks of sample FG3 measured in time, after each vibration cycle. The growth of crack number is clearly exponential.

It must be emphasized that it takes many hours for the first surface crack to appear, but the second and the next cracks appear in a short time after the first. The applied acceleration profile of 2,14m/s^2 (rms) is low compared to the profiles used in the first set of experiments (§2.3.1). The best fit for the data seen as points in the diagram is possible with the exponential curve described by the equation $y=e^{a+bx+cx2}$ (figures 10,11).

Table 6 Comparison of the two sets of samples and loading

	First set of samples	**Second set of samples**
Dimensions	60x80cm	60x80cm
Support	linen canvas, sized with warm skin glue	linen canvas, sized with warm skin glue
Layers	• Two layers of gesso • A partial black acrylic paint layer • Varnish	• Two layers of gesso
Induced defects	• adhesion gaps between the support and the gesso layers using Tricyclen-Camphen	• adhesion gaps between the support and the gesso layers using cyclododecan • Small weights (1.6g of gesso) were locally fixed on the surface
	Vibration loading	**Vibration loading**
Characteristics	Random white noise with limited bandwidth (1 to 50 Hz)	Loops of 20sec of handling (loading/unloading/trolley) and 80sec of truck transport (as recorded on real transports)
Root mean square (rms) acceleration	Increasing acceleration starting at 1m/s^2 to 10m/s^2 with a step of +1m/s^2	Standard at 2,14m /s^2

Even though the samples of the two sets have slightly different construction as presented in table 6 and the applied loading as presented in tables 2-5 is also slightly different the experimental measurements are represented by the $3p^2$ exponential curve described in the equation $y=e^{(a+bx+cx2)}$ that effectively signifies the infinitesimal increase of parameter y. In the exponential expression there is not finite growth or plateau to be reached instead the quantity as long as the cause exists reaches steadily higher values.

4. CONCLUSION

Transportation realistic simulation on known defect canvas painting samples monitored in real-time with digital holographic speckle pattern interferometry transportable system (DHSPI) have provided an adequate and successful method to reveal the transport conditions under which the first surface cracks appear and monitor the invisible yet effects of expansion and propagation. The visual qualitative raw data provided the necessary temporal window of time resolution to follow the expansion ways of cracking patterns and measure them on scale. The quantified results in terms of number of cracks at each vibration cycle proved to follow the same exponential model of growth on two different types of samples and vibration profiles. Further studying of transportation effects will contribute in the better understanding of the fracture mechanisms on canvas paintings and enhance guidelines for transportation and handling.

4. 1 Post-data discussion

Most important finding to denote from the presented experiment is the strong evidence that the experimentally resulted data is in accordance to the specific exponential function described by the equation $y=e^{a+bx+cx2}$. Under this experimental observation the crack growth and propagation of total deterioration rate of a canvas painting approaches a more regular and foreseeable way of response to vibration induced by transportation and dedicated experiments. To exploit further this behaviour and define the limits of deviation and statistical error further experiments should be planned. This may be useful to solve uncertainties in crack studies in movable artwork transportation.

Upon modelling the experimental evidence of surfacing a crack due to vibration frequency that with temporal evolution activates cracking propagation and interconnection a stochastic analysis of the cracking risk is discussed [35]. We assume cracking surface S_0 with cracks y_n that can deteriorate further with vibration frequencies v of a variety of magnitudes M_j causing extension of cracking from y_0 to y_j. For any such M_j the surface crack y_j is related to frequency v_M with attenuation $y=f(M,\Delta)$ where Δ the distance among y, y_j and $\Delta \leq \Delta_j$. Since attenuation relation is symmetrical then y_j extension is possible with $v_j=v_M\ \pi\Delta^2/S_0$. The algorithm expresses the probable extension risk y_j in excess of v magnitude. In case that the risk is focused on the cracking extent the frequency v_M is related to L_0 reference length and the algorithm is $v_j=v_M\ 2\Delta j/L_0$ for magnitude M, distance Δj and given value of y_j.

Then considering the time dependence among the vibration cycles the procedure follows the deformation rate of $\delta=d\gamma/dt$ for displacement δ among y_j cracks of surface S_0. If a characteristic vibration of magnitude M provokes displacement δ the constant rate of deterioration requests vibration repetition with mean periodicity $T= \delta/\ d\gamma/dt$ for crack y and crack length extension L. Since for reference crack length L_0 $T_M=1/v_M$, then $T=T_M\ L_0/L_j$. The above described physical mechanism of crack generation can be expressed in a model for temporal dependent since time parameter is dominant in the experiments. Hence if previous crack appeared at t=0 next crack will appear after repetition T and deviation σ of the mean value. It is schematically shown in figure 12 where it is seen the asymptotic exponential plotted result of the experimental study with its Gaussian error deviation.

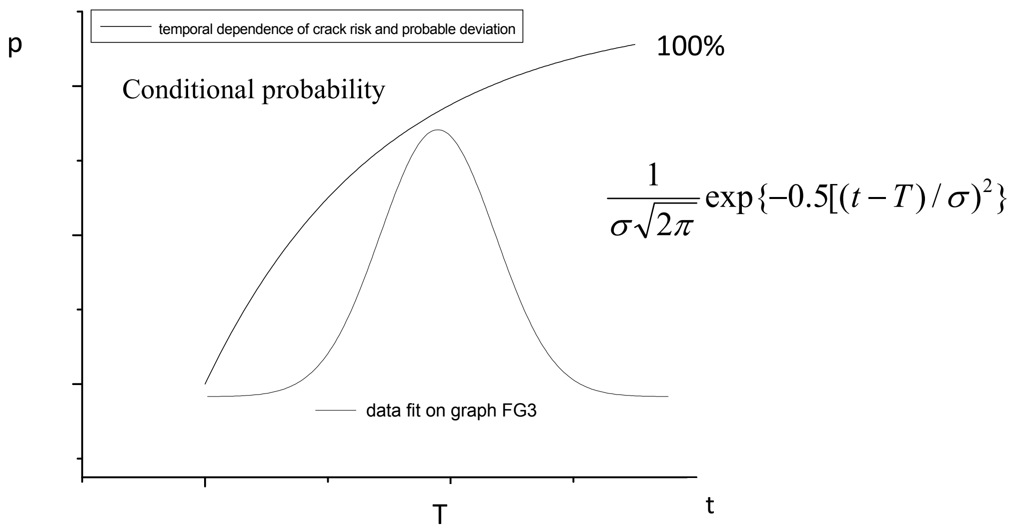

Figure 12 Temporal dependence of cracking risk with Gaussian deviation of probabilistic error.

The deviation σ of the mean repetition time can be considered as a Gaussian distribution of error deviation function,

$$f(t) = \frac{1}{\sigma\sqrt{2\pi}}\exp\{-0.5[(t-T)/\sigma)^2\} \tag{2}$$

So if the previous crack appeared on surface at time 0 the next crack will be surfaced after mean repetition T and deviation σ.

The probability condition to occur surface crack in time t_r from t to t+ Δt if there hasn't reach surface till time t,

$$p(t \le t_r < t + \Delta t) = \int_t^{t+\Delta t} f(t)dt \Big/ \int_t^{\infty} f(t)dt \tag{3}$$

For homogeneous and isotropic materials in elastic mediums the mechanical waves following the above expression could be used to classify the risk probability on a table. However the structural condition, ageing, existing defects and molecular degradation consisting the material properties and construction which affect crack deterioration and resonance or attenuation are crucial random parameters that do not allow a normalized probability distribution of crack risks to be tabled. Another important denotation is the difference between the times that the first crack takes to appear in comparison with the time of the second crack. It appears that there is a "safe" time-window in new canvas paintings without pre-existent cracks that the painting preserves its degree of elasticity and it can withstand transportation vibrations. After this "elastic" period and the appearing of first crack it is shown that the next cracks should appear much sooner and in an exponential way as proved above. The decrease of the deterioration rate after the 10^{th} cycle of figure 8 could be explained by taking account also the resonance frequency of the sample which with increase in the vibration cycles it decreases. There is a possibility that the canvas does not resonate any more with the applied acceleration profiles and thus the deterioration rate seems to decrease.

It is clear that the above denotations concern the specific type of canvas samples with induced defects and selected realistic parameters for laboratory simulations. To be able to extent the observations and arguments of the presented study and generalize safety conclusions for canvas transportation it is assumed that further research on the topic is planned.

REFERENCES

1 Green, T., ‘Shock and vibration: test results for framed paintings on canvas supports’, in ICOM Committee for Conservation, 8th Triennial Meeting, Sydney, 6-11 September 1987: Preprints, ed. K. Grinstad, The Getty Conservation Institute, Los Angeles (1987) 585-596.

2 Bäschlin, N., Läuchli, M., Fankhauser, T., Palmbach, C. and Hoess, A., ‘Backing boards and glazing on paintings: their damping capacity in relation to shock impact and vibration’, in ICOM-CC 16th Triennial Conference, Lisbon, Criterio, Lisbon (2011) S.1–S.11.

3 Erlebacher, J., D., Brown, E., Mecklenburg, M.F. and Tumosa, C., S., ‘The effects of temperature and relative humidity on the mechanical properties of modern painting materials’, Materials Research Society Proceedings **267** (1992) 359-370.

4 Young, C., and Hagan, E., ‘Cold temperatures effects on modern paints used for priming flexible supports’, in Preparation for Painting: The Artist's Choice and Its Consequences, ed. Townsend, J., H., Doherty, T., Heydenreich, G. and Ridge, J., Archetype, London **163** (2008) 71.

5 Green, T., ‘Vibration control: paintings on canvas supports’, in Art in transit: studies in the transport of paintings, National Gallery of Art, Washington DC (1991) 59–67.

6 Marcon, P.J. and Mecklenburg, M.F., ‘Shock, vibration and the shipping environment’, in Art in transit: studies in the transport of paintings, National Gallery of Art, Washington DC (1991) 121–132.

7 Michalski, S., ‘Paintings - their response to temperature, relative humidity, shock, and vibration’, in Art in transit: studies in the transport of paintings, National Gallery of Art, Washington DC (1991) 223–248.

8 Saunders, D., Leback Sitwell, C. and Staniforth, S., ‘Soft pack – the soft option?’, in Art in transit: studies in the transport of paintings, National Gallery of Art, Washington DC (1991) 311–321.

9 Caldicott, P.J. and Mecklenburg, M.F., ‘Vibration and shock in transit situations: a practical evaluation using random vibration techniques’, in Art in transit: studies in the transport of paintings, National Gallery of Art, Washington DC (1991) SE-1–SE-24.

10 Lasyk, Ł., Łukomski, M., Bratasz, Ł. and Kozłowski, R., ‘Vibration as a hazard during the transportation of canvas paintings’, in Conservation and Access, ed. D. Saunders, J.H. Townsend and S. Woodcock, IIC, London (2008) 64–68.

11 Mecklenburg, M.F., ‘Applied mechanics of materials in conservation research’, in Materials Issues in Art and Archaeology II, ed. P.B. Vandiver, J. Druzik and G.S. Wheeler, Materials Research Society, Pittsburgh **185** (1991) 105–122.

12 Targowski, P., Góra, M., Bajraszewski, T., et al., ‘Optical Coherence Tomography for Tracking Canvas Deformation’, Laser Chemistry **2006** (2006) 93658.

13 Bernikola, E., Hatzigiannakis, K., Tornari, V., Hackney, S. and Green T., ‘Effects of artificial ageing procedure on canvas model paintings monitored in micro scale’, *8th EC Conference CHRESP,* ed. J. Kolar and M. Strlič, National and university library, Ljubljana (2008) 27.

14 Groves, M.R., Osten, W., Doulgeridis, M., Kouloumpi, E., Green, T., Hackney, S. and Tornari, V., ‘Shearography as part of a multi-functional sensor for the detection of signature features in movable cultural heritage’, SPIE **6618** (2007) 661810.

15 Thizy, C., Georges, M., Doulgeridis, M., Kouloumpi, E., Green, T., Hackney, S. and Tornari, V., ‘Role of dynamic holography with photorefractive crystals in a multifunctional sensor for the detection of signature features in movable cultural heritage’, SPIE **6618** (2007) 661812.

16 Bernikola, E., Tornari, V., Nevin, A. and Kouloumpi, E., ‘Monitoring of changes in the surface movement of model panel paintings following fluctuations in relative humidity; preliminary results using digital holographic speckle pattern interferometry’, in LACONA VII, ed. J. Ruiz , R. Radvan , M. Oujja , M. Castillejo and P. Moreno, Taylor and Francis Group, London (2008) 393–397.

17 Young, C., ‘Measurement of the biaxial properties of nineteenth century canvas primings using electronic speckle pattern interferometry’, Optics and Lasers in Engineering **31** (1999) 163–170.

18 Paoletti, D., Schirripa Spagnolo, G., Facchini, M. and Zanetta, P., ‘Artwork diagnostics with fiber-optic digital speckle pattern interferometry’, Applied Optics **32** (1993) 6236–6241.

19 Hinsch, K.D., Gulker, G. and Helmers, H., ‘Checkup for aging artwork— optical tools to monitor mechanical behaviour’, Optics and Lasers in Engineering **45** (2007) 578–588.

20 Albrecht, D., Franchi, M., Lucia, A.C., Zanetta, P.M., Aldrovandi, A., Cianfanelli, T., Riitano, P., Sartiani, O. and Emmony, D.C., ‘Diagnostic of the conservation state of antique Italian paintings on panel carried out at the Laboratorio di Restauro dell’Opificio delle Pietre Dure in Florence, Italy with ESPI-based portable instrumentation’, Journal of Cultural Heritage **1** (2000) S331–S335.

21 Schirripa Spagnolo, G., Ambrosini, D. and Guattari, G., ‘Electro-optic holography system and digital image processing for in situ analysis of microclimate variation on artworks’, Journal of Optics **28** (1997) 99–106.

22 Tornari, V., ‘Laser interference-based techniques and applications in structural inspection of works of art’, Analytical and Bioanalytical Chemistry **387** (2007) 761–780.

23 Tsiranidou, E., Tornari, V., Orphanos, Y., Kalpouzos, C. and Stefanaggi, M., ‘Time-dependent defect reveal assessed by combination of laser sensing tools’, in LACONA VI, ed. J. Nimmrichter, W. Kautek and M. Schreiner, Springer Proceedings in Physics, Vienna (2005) 611–620.

24 Tornari, V., Bernikola, E., Nevin, A., Kouloumpi, E., Doulgeridis, M. and Fotakis, C., ‘Fully non contact holography-based inspection on dimensionally responsive artwork materials’, Sensors **8** (2008) 8401–8422.

25 Tornari, V., Orphanos, Y., Dabu, R., Blanaru, C., Stratan, A., Pacala, O. and Ursu, D., ‘Non-destructive speckle interferometry diagnosis method for art conservation’, SPIE **6606** (2006) 66060W.

26 Holographic Interferometry, Vest, C.M., Wiley, New York (1979).

27 Lasers in the Preservation of Cultural Heritage; Fotakis, C., Anglos, D., Zafiropulos, V., Georgiou, S. and Tornari, V., Principles and applications, Taylor and Francis, New York (2006).

28 Holographic and Speckle Interferometry Jones, R. and Wykes, C., 2nd edition, Cambridge University Press, Cambridge (1989).

29 Laser Speckle and Related Phenomena, Dainty, J.C., Springer-Verlag, Berlin (1975).

30 Dai, C., Yu, Y. and Tornari, V., ‘Electroholographic display with SLM’, SPIE **6695** (2007) 669515

31 Osten, W., Werner, P.O.J. and Mieth, U., ‘Knowledge-assisted evaluation of fringe patterns for automatic fault detection’, SPIE **2004** (1994) 256.

32 Tornari, V., Zafiropulos, V., Vainos, N.A. and Fotakis, C., ‘A holographic systematic approach to alleviate major dilemmas in museum operation’, in EVA ’98 Conference, Berlin (1998).

33 Mieth, U., Osten, W. and Juptner, W., ‘Investigations on the appearance of material faults in holographic interferograms’, in Fringe 2001, ed. W. Osten and W. Jüptner, Elsevier, Amsterdam (2001) 163–172.

34 Tornari, V., Tsiranidou, E. and Bernikola, E., ‘Interference fringe-patterns association to defect-types in artwork conservation: an experiment and research validation review’, Appl. Phys. A **106** (2012) 397-410.

35 ‘Technical Seismology”, Papastamatiou, D.I., EMP Athens Polytechnic University Student press, Athens (1997).

List of figure captions

Figure 1 Photograph of the DHSPI monitoring system and transport simulator set up.

Figure 2 (a) Schematic of a sample. Circles indicate the location of weak spots. (b) Schematic of the construction of the sample.

Figure 3 Schematic of canvas sample with known structural defects on the sample.

Figure 4 Vibration profile of rms = 2,14m/s2.

Figure 5 Schematic representation of the experimental measuring methodology.

Figure 6. Example of local crack map registered from interferograms after 10th vibration cycle at t=100 min, in a) crack map resulted from interferograms of sample TP1, propagation length marked in red, and b) the known defect map.

Figure 7 Total number of cracks measured after each vibration cycle. The crack growth is exponential.

Figure 8 Deterioration rate of the test painting measured in number of new cracks generated after each vibration cycle. The rate decreases after the 10th cycle.

Figure 9 Example of interferograms, a) reference interferogram -before vibration loading- of sample FG2 according to the sample construction shown in figure 3, b) after 1st vibration cycle at t=30 min. Orange arrows show potential yet hidden cracks. Red arrow shows the first surface crack that appeared after 7th vibration cycle at t=810 min, c) with red arrows indicating the full length of the crack, d) FG2 after 9th vibration cycle and at t= 890 min, e) zoom-in surface crack map studied from interferograms of sample FG2 showing the first two surface cracks and f) zoom-in known defect map.

Figure 10 Number of surface cracks of samples FG1 and FG2 measured in time, after each vibration cycle. The growth of crack number is clearly exponential.

Figure 11 Number of surface cracks of sample FG3 measured in time, after each vibration cycle. The growth of crack number is clearly exponential.

Figure 12 Temporal dependence of cracking risk with Gaussian deviation of probabilistic error.

List of table captions

Table 1 Experimental Procedure